

## Kinetic isotope effects of $^{12}\text{CH}_3\text{D} + \text{OH}$ and $^{13}\text{CH}_3\text{D} + \text{OH}$ from 278 to 313 K

L. M. T. Joelsson<sup>1,3</sup>, J. A. Schmidt<sup>1</sup>, E. J. K. Nilsson<sup>2</sup>, T. Blunier<sup>3</sup>, D. W. T. Griffith<sup>4</sup>, S. Ono<sup>5</sup>, and M. S. Johnson<sup>1</sup>

<sup>1</sup>Department of Chemistry, University of Copenhagen, Copenhagen, Denmark

<sup>2</sup>Division of Combustion Physics, Department of Physics, Lund University, Sweden

<sup>3</sup>Centre for Ice and Climate (CIC), Niels Bohr Institute, University of Copenhagen, Copenhagen, Denmark

<sup>4</sup>University of Wollongong, Department of Chemistry, Wollongong, Australia

<sup>5</sup>Department of Earth, Atmospheric and Planetary Sciences, Massachusetts Institute of Technology, Cambridge, MA, USA

Correspondence to: M. S. Johnson (msj@kiku.dk)

**Abstract.** Methane is the second most important long lived greenhouse gas and plays a central role in the chemistry of the Earth's atmosphere. Nonetheless there are significant uncertainties in its source budget. Analysis of the isotopic composition of atmospheric methane, including doubly substituted species (e.g.  $^{13}\text{CH}_3\text{D}$ ), offers new constraints on the methane budget as the sources and  
5 sinks have distinct isotopic signatures. The most important sink of atmospheric methane is oxidation by OH in the troposphere which accounts for around 84% of all methane removal. Here we present experimentally derived methane + OH kinetic isotope effects and their temperature dependence over the range of 278 to 313 K for  $\text{CH}_3\text{D}$  and  $^{13}\text{CH}_3\text{D}$ ; the latter is reported here for the first time. We find  $k_{\text{CH}_4}/k_{\text{CH}_3\text{D}} = 1.31 \pm 0.01$  and  $k_{\text{CH}_4}/k_{^{13}\text{CH}_3\text{D}} = 1.34 \pm 0.03$  at room temperature, implying that  
10 the methane + OH kinetic isotope effect is multiplicative such that  $(k_{\text{CH}_4}/k_{^{13}\text{CH}_4})(k_{\text{CH}_4}/k_{\text{CH}_3\text{D}}) = k_{\text{CH}_4}/k_{^{13}\text{CH}_3\text{D}}$ , within the experimental uncertainty, given the literature value of  $k_{\text{CH}_4}/k_{^{13}\text{CH}_4} = 1.0039 \pm 0.0002$ . In addition, the kinetic isotope effects were characterized using transition state theory with tunneling corrections. Good agreement between the experimental, quantum chemical, and available literature values was obtained. The theoretical calculation confirms that the  $^{13}\text{CH}_3\text{D}$   
15 isotope effect is the product of D- and  $^{13}\text{C}$ - isotope effects. Based on the results we conclude that the OH reaction (the main sink of methane) at steady-state can produce an atmospheric clumped isotope signal ( $\Delta(^{13}\text{CH}_3\text{D}) = \ln([\text{CH}_4][^{13}\text{CH}_3\text{D}]/[^{13}\text{CH}_4][\text{CH}_3\text{D}])$ ) of  $0.02 \pm 0.02$ .

## 1 Introduction

Atmospheric methane is the subject of increasing interest from both the climate research community and the public due its impacts on climate change, as reported by the IPCC (2013). The direct radiative forcing of methane is  $0.64 \text{ Wm}^{-2}$ . Including feedback mechanisms and secondary effects e.g. increased  $\text{O}_3$  production, stratospheric water vapor and production of  $\text{CO}_2$ , methane's radiative forcing becomes  $0.97 \text{ Wm}^{-2}$ , 2/3 of the forcing by  $\text{CO}_2$  over the same time period (IPCC, 2013, Fig. 8.15).

Atmospheric methane has both natural and anthropogenic sources and the two categories contribute about equally (Ciais et al., 2013, and references therein). Wetlands are the dominant natural source, and agriculture and waste are the largest anthropogenic sources. Fossil fuels make smaller contributions. A majority (84%) of atmospheric methane is removed by oxidation by OH in the troposphere:



oxidation in the troposphere by Cl contributes about 4% of the total:



About 8% of methane is removed in the stratosphere by radical oxidation, such as reactions (R2) and (R3):



The rest (4%) is removed by soil (Kirschke et al., 2013).

Carbon and hydrogen isotopic analysis are widely used to distinguish microbial and thermal sources of atmospheric methane (e.g., Lowe et al., 1997; Ferretti et al., 2005; Tyler et al., 2007; Lassey et al., 2007). However, reactions (R1), (R2), and (R3) produce relatively large D/H isotope effects (Saueressig et al., 1995, 1996, 2001; Crowley et al., 1999; Feilberg et al., 2005). Thus, the construction of an accurate top-down methane budget by isotopic analysis, must take the isotopic signatures of both sources and sinks into account (Quay et al., 1999; Bergamaschi et al., 2000; Allan et al., 2001a, b). An isotope budget based on methane source (and sink) fractionations result in an underdetermined systems (e.g., Pohlman et al., 2009). Recent advances in mass spectrometry (Eiler et al., 2013; Stolper et al., 2014) and laser infrared spectroscopy (Ono et al., 2014; Wang et al., 2015) facilitate measurement of rare double-substituted isotopologues. The abundance of these "clumped" isotopologues (clumped refers to the rare isotopes being clumped together) generally follows a stochastic distribution (i.e.  $[{}^{12}\text{CH}_4][{}^{13}\text{CH}_3\text{D}] = [{}^{13}\text{CH}_4][{}^{12}\text{CH}_3\text{D}]$ ). However, small deviations from stochastic distribution can be induced by thermodynamic (Ma et al., 2008; Stolper et al., 2014; Liu and Liu, 2016), kinetic (Joelsson et al., 2014; Wang et al., 2015), and photolytic processes (Schmidt et al., 2013; Schmidt and Johnson, 2015). Analysis of the clumped isotope anomaly in

methane will yield unique constraints for the methane budget. Optical methods, as will be shown in this paper, provide high throughput and accuracy for overcoming the problems of analysis of clumped  $\text{CH}_4$ . The difference and advantage of this approach is the additional information not available in single isotope analysis, especially regarding the mechanism of formation, independent of the enrichment of D and  $^{13}\text{C}$  in the starting material.

The kinetic isotope effect  $^j\text{E}_\alpha$  is a characteristic property of each process:

$$^j\text{E}_\alpha \equiv \frac{k(^i\text{E} + \text{OH})}{k(^j\text{E} + \text{OH})}, \quad (1)$$

where  $^i\text{E}$  is the most abundant (here, the lighter) isotopologue,  $^j\text{E}$  the rare (heavy) isotopologue,  $k(\text{E} + \text{OH})$  is the reaction rate coefficient for the reaction  $\text{E} + \text{OH}$ . As a measure of how much of a fractionation of  $^{13}\text{CH}_3\text{D}$  kinetic reactions produce, the apparent clumpiness,  $\gamma$  is used. It is a measure of the effect of the clumped substitution on the reaction rate, as opposed to the combined effect of two single substitutions. It is defined as (Wang et al., 2015):

$$\gamma \equiv \frac{^{13}\text{C},\text{D}_\alpha}{^{13}\text{C}_\alpha \times \text{D}_\alpha} \quad (2)$$

A related measure is the  $\Delta(^{13}\text{CH}_3\text{D})$  value that quantifies the extent to which rare isotopes clump together to form a multiply substituted species, as opposed to a stochastic distribution (Ono et al., 2014):

$$\Delta(^{13}\text{CH}_3\text{D}) \equiv \ln \left( \frac{[^{13}\text{CH}_3\text{D}][^{12}\text{CH}_4]}{[^{12}\text{CH}_3\text{D}][^{13}\text{CH}_4]} \right), \quad (3)$$

where  $[^{13}\text{CH}_3\text{D}]$ ,  $[^{12}\text{CH}_4]$ ,  $[^{12}\text{CH}_3\text{D}]$  and  $[^{13}\text{CH}_4]$  represent the concentrations of the different isotopologues.

The kinetic isotope effects for the singly substituted species  $\text{CH}_3\text{D}$  and  $^{13}\text{CH}_4$  have been studied previously both experimentally and theoretically, see Tables 3 and 4 respectively. The kinetic isotope effect  $^{13}\text{C},\text{D}_\alpha$  for the reaction with OH is not described in the existing literature. The related kinetic isotope effect for the  $\text{CH}_4 + \text{Cl}$  reaction was measured at room temperature with the present setup by Joelsson et al. (2014) and found to be  $1.60 \pm 0.04$ .

In the present study the kinetic isotope effects  $\text{D}_\alpha$  and  $^{13}\text{C},\text{D}_\alpha$  are determined using the relative rate method. Species concentrations in the reaction cell are determined using Fourier Transform Infrared (FTIR) spectroscopy. Further,  $\text{D}_\alpha$ ,  $^{13}\text{C}_\alpha$ , and  $^{13}\text{C},\text{D}_\alpha$  are calculated using quantum chemistry and transition state theory.

## 2 Experimental procedures

Sixteen experiments were conducted, numbered from 1 through 16, see Table 1; eight (Experiments 1–8) for  $^{12}\text{CH}_3\text{D}$  and eight (Experiments 9–16) for  $^{13}\text{CH}_3\text{D}$ . The experiments were conducted at

four different temperatures ( $T = [298, 278, 288, 313]K = [25, 5, 15, 40]^\circ C$ ); two experiments were conducted for each temperature.

## 85 2.1 Relative rate method

The experiments were carried out using the relative rate method on a semi-static gas mixture. The decaying concentrations of reactants were measured as a function of the extent of reaction. Considering two bimolecular reactions with second order rate coefficients  $k_A$  and  $k_B$ ,



and assuming there were no other loss processes, the following relation holds:

$$\ln \left( \frac{[A]_0}{[A]_t} \right) = \frac{k_A}{k_B} \ln \left( \frac{[B]_0}{[B]_t} \right). \quad (4)$$

Here  $[A]_0$ ,  $[A]_t$ ,  $[B]_0$  and  $[B]_t$  represent the concentrations of compounds A and B at times 0 and  $t$  respectively. The slope of  $\ln([A]_0/[A]_t)$  versus  $\ln([B]_0/[B]_t)$  gives the relative reaction rate coefficient. In these experiments A is  $^{12}\text{CH}_4$  and B is  $^{12}\text{CH}_3\text{D}$  or  $^{13}\text{CH}_3\text{D}$ .

## 2.2 Photoreactor

Experiments were carried out in the photochemical reactor at the University of Copenhagen, Department of Chemistry. The reactor has been described in detail elsewhere (Nilsson et al., 2009). It consists of a 100 L quartz cell with multi-pass optics surrounded by 16 UV-C fluorescent Hg lamps  
100 in a temperature controlled housing. The cell is coupled to a Bruker IFS 66v/S FTIR spectrometer with either a mercury cadmium telluride (MCT) detector (Experiments 1–4) or an indium antimonide (InSb) (Experiments 5–16). The InSb-detector has a better signal-to-noise ratio, the MCT-detector is used in Experiments 1–4 for logistical reasons. Two thermocouple gauges are placed inside the temperature controlled housing to monitor the temperature and a pressure gauge is connected to the  
105 cell to monitor pressure inside the cell. The temperatures and the pressures were logged every 0.5 s.

## 2.3 Laboratory procedure

Gas mixes were prepared by expanding  $\text{H}_2\text{O}$  vapor (Milli-Q Ultrapure Water) into the chamber through a glass gas manifold. The two methane isotopologues  $\text{CH}_3\text{D}$  (Experiments 1–8) (purity > 98%, Cambridge Isotope Laboratories, Inc.) or  $^{13}\text{CH}_3\text{D}$  (Experiments 9–16), and  $\text{CH}_4$  (purity  
110 > 99%, Aldrich) and  $\text{O}_3$  were flushed into the chamber with a  $\text{N}_2$  buffer (purity 99.998%, Air Liquide), all at the concentrations given in Table 1.  $^{13}\text{CH}_3\text{D}$  was synthesized using the Grignard

reaction, see Joelsson et al. (2014).  $O_3$  was generated from  $O_2$  (purity 99.97 %, Air Liquide) using an ozone generator (Model AC-20,  $O_3$  Technology), preconcentrated before injection on silica gel cooled with ethanol and dry ice to  $-67^\circ\text{C}$ . The desired pressure in the cell (450 hPa) was obtained  
115 using  $N_2$  as bath gas. The starting pressure is chosen such that the pressure is high enough for the  $N_2$  to quench  $O(^1D)$  radicals, but low enough to keep the final pressure below atmospheric pressure. The gas mixture was left to rest for up to 1.5 hours while several IR spectra were recorded to ensure that no instability or dark chemistry occurs in the gas mix. The UV-C lamps were lit for up to 5 min photolysing at least 75 % of the  $O_3$  according to:



$O(^1D)$  then subsequently reacts with  $H_2O$  to yield OH:



Up to 0.2 Pa  $O_3$  was flushed with about 20 hPa  $N_2$  into the chamber to compensate for the loss of ozone with time, mainly due to  $O(^3P) + O_3$ . A pressure gradient was established and maintained  
125 throughout the filling process such that no gas leaked back from the chamber into the gasline. Spectra were recorded at each filling step. The procedure was repeated until the mix had a final pressure of 933 hPa. Two experiments were conducted at each of the temperatures 278, 288, 298, and 313 K for each of the two heavy methane isotopologues. Exact temperatures are listed in Table 1. After each experiment a dilution test was performed: 133 hPa was pumped out and the chamber is refilled with  
130 133 hPa  $N_2$ . This was repeated 5–6 times. Ideally, concentration calculations from the spectral fits (data analysis described below) of the resulting spectra should give a linear fit with the slope of 1. The slope of these dilution tests are presented in Table 2. In an extra experiment with  $^{12}\text{CH}_3\text{D}$ ,  $N_2O$  (Air Liquide, no purity information available) was added as an  $O(^1D)$  tracer. The results from this experiment are used as a benchmark to validate a model that was constructed to investigate the extent  
135 of  $O(^1D)$  chemistry, see Sect. 2.5. An example of an experimental plot can be found in Fig. 4 and the full data set in Figs. S1–S8 in the Supplement.

## 2.4 Data analysis

The experimental IR spectra were analyzed using the program MALT which simulates experimental FTIR spectra (Griffith, 1996) combined with non-linear least squares fitting to best-fit the calculated  
140 spectra to measured spectra (Griffith et al., 2012). The MALT program generates a simulated spectrum from initial estimates of the absorber concentrations and instrument parameters. The residual between the experimental and simulated spectra is reduced through iteration. Simulated line-shapes are generated using HITRAN absorption parameters (version 2008) (Rothman et al., 2009) convolved with an FTIR instrument function simulating the Bruker IFS 66v/S instrument. The InSb  
145 detector covers a spectral range from  $1800\text{--}5000\text{ cm}^{-1}$  and the MCT detector covers a spectral

**Table 1.** Experimental setup. The experiment numbers are listed in column Exp., the detector in the column Detect., the heavy CH<sub>4</sub> isotopologue included in the experiments are listed in column [<sup>x</sup>CH<sub>3</sub>D], the mean measured temperatures in the photoreactor are listed in column *T*, the H<sub>2</sub>O-vapour concentrations at the start of the experiments (*t* = 0) as obtain from spectral fitting are listed in column [H<sub>2</sub>O]<sub>*t*=0</sub>, the mean O<sub>3</sub> concentration after refill (i.e. the “top”-values) as obtain from spectral fitting are listed in column [O<sub>3</sub>]<sub>top</sub>, the <sup>12</sup>CH<sub>4</sub>- concentrations at the start of the experiments (*t* = 0) as obtain from spectral fitting are listed in column [<sup>12</sup>CH<sub>4</sub>]<sub>*t*=0</sub>, and the heavy CH<sub>4</sub> concentrations at the start of the experiments (*t* = 0) as obtain from spectral fitting are listed in column [<sup>x</sup>CH<sub>3</sub>D]<sub>*t*=0</sub>. Note that for the experiment including CH<sub>3</sub>D, the value of initial concentration only refers to [<sup>12</sup>CH<sub>3</sub>D]<sub>*t*=0</sub>.

Exp.	Detect.	<sup>x</sup> CH <sub>3</sub> D	<i>T</i> /K	[H <sub>2</sub> O] <sub><i>t</i>=0</sub> /hPa	[O <sub>3</sub> ] <sub>top</sub> /hPa	[ <sup>12</sup> CH <sub>4</sub> ] <sub><i>t</i>=0</sub> /hPa	[ <sup>x</sup> CH <sub>3</sub> D] <sub><i>t</i>=0</sub> /hPa
1	MCT	CH <sub>3</sub> D	298.2 ± 1.2	7.1	– <sup>a</sup>	0.030	0.054
2	MCT	CH <sub>3</sub> D	297.6 ± 0.8	5.6	0.19	0.058	0.042
3	MCT	CH <sub>3</sub> D	277.2 ± 0.2	5.2	0.29	0.109	0.046
4	MCT	CH <sub>3</sub> D	277.0 ± 0.2	5.1	0.16	0.073	0.035
5	InSb	CH <sub>3</sub> D	284.5 ± 0.1	7.2	0.26	0.025	0.033
6	InSb	CH <sub>3</sub> D	291.1 ± 0.2	7.4	– <sup>a</sup>	0.052	0.050
7	InSb	CH <sub>3</sub> D	313.5 ± 1.3	7.1	0.17	0.025	0.029
8	InSb	CH <sub>3</sub> D	312.4 ± 0.9	4.3	– <sup>a</sup>	0.022	0.040
9	InSb	<sup>13</sup> CH <sub>3</sub> D	298.5 ± 0.1	5.1	– <sup>a</sup>	0.035	0.026
10	InSb	<sup>13</sup> CH <sub>3</sub> D	297.6 ± 0.6	6.4	0.13	0.025	0.033
11	InSb	<sup>13</sup> CH <sub>3</sub> D	276.8 ± 0.8	5.4	– <sup>a</sup>	0.024	0.024
12	InSb	<sup>13</sup> CH <sub>3</sub> D	277.2 ± 1.3	5.1	– <sup>a</sup>	0.022	0.030
13	InSb	<sup>13</sup> CH <sub>3</sub> D	287.4 ± 1.2	5.4	– <sup>a</sup>	0.021	0.028
14	InSb	<sup>13</sup> CH <sub>3</sub> D	287.4 ± 0.4	4.5	– <sup>a</sup>	0.016	0.029
15	InSb	<sup>13</sup> CH <sub>3</sub> D	314.4 ± 1.0	5.2	0.26	0.023	0.037
16	InSb	<sup>13</sup> CH <sub>3</sub> D	313.8 ± 0.8	8.3	0.17	0.025	0.035

<sup>a</sup>Spectra recorded during or after photolysis, [O<sub>3</sub>]<sub>top</sub> not available

range from 400–5000 cm<sup>−1</sup>. The concentrations of <sup>12</sup>CH<sub>3</sub>D and <sup>13</sup>CH<sub>3</sub>D were calculated from spectral fits in the region 2140–2302 cm<sup>−1</sup>, see Fig. 1 and 2. Interference from H<sub>2</sub>O, CO<sub>2</sub>, and CO was eliminated by including simulated spectra obtained from the HITRAN database in the fit. As there is no HITRAN data available for <sup>13</sup>CH<sub>3</sub>D in this region, the cross sections from 2000–2400  
150 cm<sup>−1</sup> for this isotopologue were estimated by shifting the spectrum of <sup>12</sup>CH<sub>3</sub>D, see Joelsson et al. (2014). Concentrations of <sup>12</sup>CH<sub>4</sub> were calculated from spectral fits in the region 2838–2997 cm<sup>−1</sup>. Interference from <sup>13</sup>CH<sub>3</sub>D was reduced by including temperature adjusted reference spectra in the fit, and interference from <sup>12</sup>CH<sub>3</sub>D, H<sub>2</sub>O, and H<sub>2</sub>CO was by including simulated spectra obtained

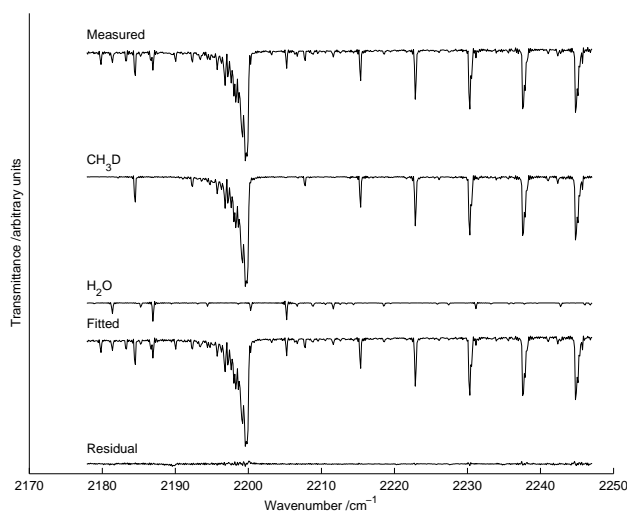


**Figure 1.** A typical spectral fit in the region where [ $^{12}\text{CH}_3\text{D}$ ] is obtained (Experiment 5). Experimental data are shown by the topmost line, followed by the fitted (synthetic) partial spectra of the most dominant absorbers ( $\text{CH}_3\text{D}$  and  $\text{H}_2\text{O}$ ), the resulting fitted (synthetic) spectrum (also including  $\text{CO}_2$  and  $\text{CO}$ ), and the residual between the measured and fitted spectra is shown by the bottom line.

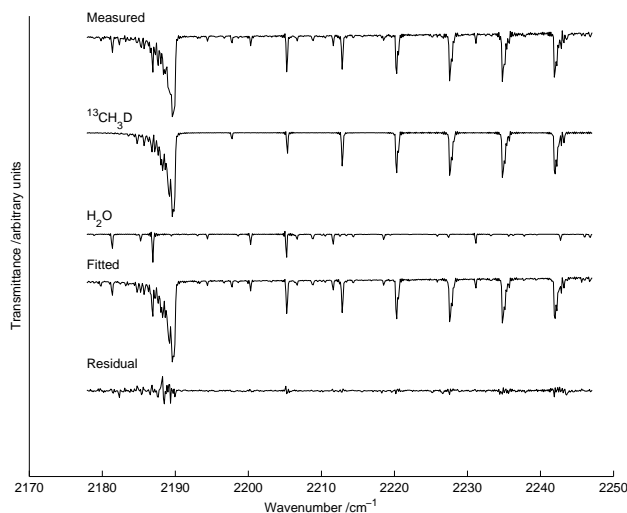


**Figure 2.** A typical spectral fit in the region where [ $^{13}\text{CH}_3\text{D}$ ] is obtained (Experiment 10). Experimental data are shown by the topmost line, followed by the fitted (synthetic) partial spectra of the most dominant absorbers ( $^{13}\text{CH}_3\text{D}$  and  $\text{H}_2\text{O}$ ), the resulting fitted (synthetic) spectrum (also including  $\text{CO}_2$  and  $\text{CO}$ ), and the residual between the measured and fitted spectra is shown by the bottom line.

from the HITRAN database in the fit, see Fig. 3. The spectral windows were sometimes adjusted to  
 155 exclude saturated lines.

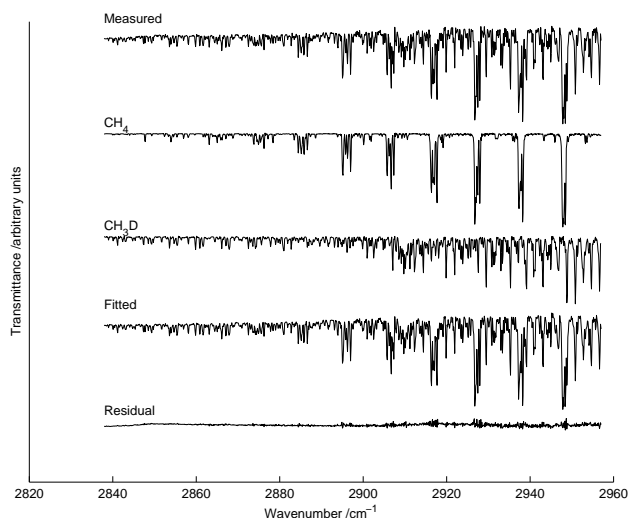


**Figure 3.** A typical spectral fit in the region where  $[^{12}\text{CH}_4]$  is obtained (Experiment 5). Experimental data are shown by the topmost line, followed by the fitted partial (synthetic) spectra of the most dominant absorbers ( $\text{CH}_4$  and  $\text{CH}_3\text{D}$ ), the resulting fitted (synthetic) spectrum (also including  $\text{H}_2\text{O}$ ), and the residual between the measured and fitted spectra is shown by the bottom line.

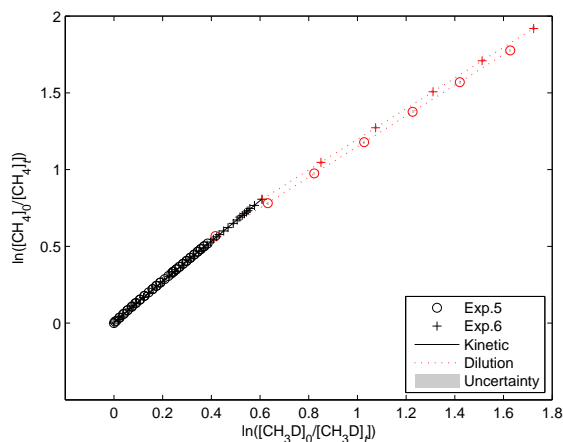


**Figure 4.** A typical experimental outcome, Experiment 5 and 6:  $\text{CH}_3\text{D}$ ,  $T = 288\text{K}$ . Experimental data are shown using black open circles (Exp. 5) and black plus signs (Exp. 6). Corresponding dilution test points are shown using red symbols. A linear fit of the experimental points is shown using a black solid line and linear fit of the subsequent dilution test are represented by a red dotted line, uncertainties for each point are represented by gray areas.

After  $[^x\text{CH}_3\text{D}]$  (where  $x = 12$  or  $x = 13$ ) and  $[^{12}\text{CH}_4]$  were obtained from the spectral analysis,  $\ln([^x\text{CH}_3\text{D}]_0/[^x\text{CH}_3\text{D}]_t)$  was plotted against  $\ln([^{12}\text{CH}_4]_0/[^{12}\text{CH}_4]_t)$  as described in Sect. 2.1. A straight line was fitted to these data points using a weighted total least squares routine (York et al.,



2004). The fitting procedure takes uncertainties in both dimensions into account. The uncertainty  
 160  $\sigma(\ln([A]_0/[A]_t))$  was calculated using standard error propagation:

$$\sigma(\ln([A]_0/[A]_t)) = \sqrt{\left(\frac{\sigma([A]_0)}{[A]_0}\right)^2 + \left(\frac{\sigma([A]_t)}{[A]_t}\right)^2} \quad (5)$$

where  $\sigma([A])$  was obtained as output from MALT. The fitting procedure, performed using a MAT-  
 LAB script (York et al., 2004), also yields an error estimation which is defined as the uncertainty of  
 the kinetic isotope effect  $\sigma(\alpha)$ . An example of a straight line fit can be found in Fig. 4 and the full  
 165 data set in Figs. S1–S8 in the Supplement. In the temperature dependence curve fitting procedure,  
 the parameters  $A$  and  $B$  are from a linearized version of the Arrhenius equation:

$$\ln(k) = \ln(A) + B \cdot T^{-1} \quad (6)$$

are adjusted to match experimental. Also here, the method of York et al. (2004) was used. The  
 temperature in the cell was taken as the spatial average of the measurements from two thermocouples  
 170 inside the temperature housing. The experiment temperature was defined by the temporal mean  
 of the spatially averaged temperature measurement series and the uncertainty of the experiment  
 temperature was the standard deviation of the spatially averaged temperature measurement series.

## 2.5 Kinetic model

A kinetic model was used to determine the influence of  $O(^1D)$ , reaction (R3), which rivals Reac-  
 175 tion (R1). The model is previously described and was used by Nilsson et al. (2012). However, only  
 the methane reaction subset and associated ( $O_x$  and  $HO_x$ ) chemistry were used here. The Kintecus  
 program (Ianni, 2003), simulates the photolysis of  $O_3$  and the following oxidation chain of  $CH_4$ . To  
 model ozone photolysis accurately, the modeled  $O_3$  was matched to the measured value by adjusting  
 the photolysis rate, then the model was verified by comparing the decrease of  $CH_4$  and the increase  
 180 of  $H_2O$  during the experiment. The model was run for each refill of  $O_3$ , where the reaction rates of  
 Reactions (R1) and (R3) were obtained. The model was designed for room temperature; experiments  
 at other temperatures were not modeled. Experiment 2 was thus modeled: 4.4% of  $CH_4$  was esti-  
 mated to be lost to Reaction (R3). In an additional experiment  $N_2O$  was introduced in the chamber  
 as an  $O(^1D)$ -tracer. Since  $N_2O$  does not react with OH and is not photolyzed at the wavelengths  
 185 present (Nilsson et al., 2009), the decreased of  $N_2O$  should be only due to Reaction (R8):



The amount of  $CH_4$  lost by reaction (R3) can therefore be approximated by:

$$1 - \frac{[CH_4]_t}{[CH_4]_0} = 1 - \exp(-k_{(R3)}[O(^1D)]t) = 1 - \frac{[N_2O]_t}{[N_2O]_0}^{(k_{(R8)}/k_{(R3)})}, \quad (7)$$

where  $k_{(R8)} = 1.27 \times 10^{-10} \text{cm}^{-3} \text{s}^{-1}$  and  $k_{(R3)} = 1.75 \times 10^{-10} \text{cm}^{-3} \text{s}^{-1}$  (Sander et al., 2010). This gives 2.3%  $[\text{CH}_4]$  lost by oxidation of  $\text{O}(^1\text{D})$ , Reaction (R3). The kinetic model described above estimated that 4.7 %  $[\text{CH}_4]$  were lost by Reaction (R3) for this additional experiment. Both methods agree that  $\text{O}(^1\text{D})$  loss is a minor channel. No correction is applied, and the possible deviation is included in the estimated error.

### 3 Theoretical procedure

Rate constants and kinetic isotope effects for  $\text{CH}_4 + \text{OH}$  were calculated using a procedure similar to that employed by Joelsson et al. (2014).

#### 3.1 Computational chemistry calculations

The geometries of reactants, products and transition states were determined using a geometry optimization procedure based on the unrestricted MP2 method (Møller and Plesset, 1934) and the aug-cc-pVQZ orbital basis set (Dunning Jr., 1989; Woon and Dunning Jr., 1993). Harmonic vibrational frequencies for all relevant isotopologues of reactants, products, and transition states were obtained at the same level of theory. The calculations were carried out using the Gaussian 09 program package (Frisch et al., 2009).

The electronic energy of the optimized structures were refined using the CCSD(T) method (Watts et al., 1993; Knowles et al., 1993, 2000) with aug-cc-pVTZ, aug-cc-pVQZ, and aug-cc-pV5Z basis sets. The results from the different basis sets were used to extrapolate the electronic energy at the complete basis set limit following the approach of Halkier et al. (1998) as described by Joelsson et al. (2014).

#### 3.2 Rate constant calculations

The abstraction of a  $\text{CH}_4$  hydrogen atom by OH can occur at four different sites. Depending on the methane isotopologue in question, these sites are either distinguishable or indistinguishable. Microscopic rate constants are calculated for hydrogen abstraction at each site using classical transition state theory with a tunneling correction factor,

$$k_{\text{micro}}^{(i)} = \eta_{\text{tun}}^{(i)} \frac{k_b T}{h} \frac{Q_{\text{TS}}^{(i)}}{Q_{\text{react}}^{(i)}} \exp(-\Delta E^{(i)}/RT) \quad (8)$$

where  $\Delta E^{(i)}$  is the reaction barrier height (including the zero point vibrational energy) for the  $i$ 'th reaction path.  $\eta_{\text{tun}}^{(i)}$  is a tunneling correction factor obtained using the Wigner tunneling correction (Wigner, 1932).  $Q_{\text{TS}}^{(i)}$  and  $Q_{\text{react}}^{(i)}$  are the partition functions for the transition state and reacting pair, respectively. The total rate constant is obtained by summing over the microscopic rate constants.

**Table 2.** Results. The experiment numbers are listed in column Exp., the heavy CH<sub>4</sub> isotopologue included in the experiments are listed in column <sup>x</sup>CH<sub>3</sub>D, the mean measured temperatures in the photoreactor are listed in column *T*, the kinetic isotope effect corresponding to the isotopologue are listed in column  $\alpha$ , and the result of the dilution experiments are listed in column  $k_{\text{dil}}$ .

Exp.	<sup>x</sup> CH <sub>3</sub> D	<i>T</i> /K	$\alpha$	$k_{\text{dil}}$
1	CH <sub>3</sub> D	298.2 ± 1.2	1.302 ± 0.038	1.011 ± 0.048
2	CH <sub>3</sub> D	297.6 ± 0.8	1.314 ± 0.020	– <sup>a</sup>
3	CH <sub>3</sub> D	277.2 ± 0.2	1.294 ± 0.017	0.962 ± 0.037
4	CH <sub>3</sub> D	277.0 ± 0.2	1.335 ± 0.017	– <sup>a</sup>
5	CH <sub>3</sub> D	284.5 ± 0.1	1.334 ± 0.012	0.999 ± 0.009
6	CH <sub>3</sub> D	291.1 ± 0.2	1.323 ± 0.010	0.998 ± 0.010
7	CH <sub>3</sub> D	313.5 ± 1.3	1.301 ± 0.007	1.006 ± 0.031
8	CH <sub>3</sub> D	312.4 ± 0.9	1.338 ± 0.010	– <sup>a</sup>
9	<sup>13</sup> CH <sub>3</sub> D	298.5 ± 0.1	1.359 ± 0.022	1.000 ± 0.029
10	<sup>13</sup> CH <sub>3</sub> D	297.6 ± 0.6	1.314 ± 0.007	0.990 ± 0.064
11	<sup>13</sup> CH <sub>3</sub> D	276.8 ± 0.8	1.357 ± 0.046	1.016 ± 0.031
12	<sup>13</sup> CH <sub>3</sub> D	277.2 ± 1.3	1.344 ± 0.013	1.008 ± 0.030
13	<sup>13</sup> CH <sub>3</sub> D	287.4 ± 1.2	1.346 ± 0.025	1.009 ± 0.022
14	<sup>13</sup> CH <sub>3</sub> D	287.4 ± 0.4	1.342 ± 0.015	1.011 ± 0.019
15	<sup>13</sup> CH <sub>3</sub> D	314.4 ± 1.0	1.316 ± 0.016	1.003 ± 0.038
16	<sup>13</sup> CH <sub>3</sub> D	313.8 ± 0.8	1.331 ± 0.033	1.001 ± 0.034

<sup>a</sup>No dilution test performed

## 4 Results and Discussion

220 The results of the 16 individual experiments (eight for each isotopologue) are tabulated in Table  
 2. The resulting <sup>D</sup> $\alpha$ , <sup>13</sup>C $\alpha$ , and <sup>13</sup>C,<sup>D</sup> $\alpha$  values from the experimental and theoretical studies are  
 tabulated in Tables 3, 4, and 5 along with previous experimental and theoretical results. The results  
 are also shown in Fig. 5 and 6 for reactions of CH<sub>3</sub>D and <sup>13</sup>CH<sub>3</sub>D respectively.

The exponential curve fits yielded the parameters presented in Tables 3 and 5 giving <sup>D</sup> $\alpha_{\text{Arr}} =$   
 225 1.32 ± 0.13 and <sup>13</sup>C,<sup>D</sup> $\alpha_{\text{Arr}} = 1.32 ± 0.20$  at *T* = 298K. The mean of results of room temperature  
 experiments Experiments 1 and 2, and Experiments 9 and 10 is <sup>D</sup> $\alpha_{\text{exp}} = 1.31 ± 0.01$  and <sup>13</sup>C,<sup>D</sup> $\alpha_{\text{exp}} =$   
 1.34 ± 0.03 respectively. It follows that  $\gamma_{\text{exp}} = 1.02 ± 0.02$  at *T* = 298K, using <sup>13</sup>C $\alpha_{\text{exp}} = 1.0039 ±$   
 0.0002 (Saueressig et al., 2001), meaning that the clumped isotope might react slower relative to  
 what would be predicted based on the kinetic isotope effects of CH<sub>3</sub>D and <sup>13</sup>CH<sub>4</sub>. However, if the  
 230 Arrhenius parameters are used to calculate the kinetic isotope effects at *T* = 298K,  $\gamma_{\text{Arr}} = 1.00 ± 0.18$   
 (i.e. the reaction has no clumping effect). All uncertainties are given as one standard deviation ( $\sigma$ ).  
 The theoretical results gives  $\gamma_{\text{theory}} = 1.00$  at *T* = 298K.

**Table 3.** Experimental and theoretical studies of  ${}^D\alpha$ . The temperature dependence studies are presented in the Arrhenius form  ${}^D\alpha(T) = A(T/298\text{K})^n \exp(BT^{-1})$ , where  $A$ ,  $n$ , and  $B$  are tabulated,  $T$  is the given temperature range, and  ${}^D\alpha(T = 298\text{K})$  is the resulting kinetic isotope effect at  $T = 298\text{K}$ . Where no  $B$  coefficient is presented  $A$  can be taken as  ${}^D\alpha(T)$  for the given temperature range. All uncertainties are given as one standard deviation ( $\sigma$ ).

Study	$A$	$n$	$B/\text{K}$	$T/\text{K}$	${}^D\alpha(T = 298\text{K})$
Experimental studies					
Present study <sup>a</sup>	$1.23 \pm 0.08$	0	$21 \pm 21$	[278,313]	$1.31 \pm 0.01^h$
Saueressig et al. (2001) <sup>b</sup>	$1.294 \pm 0.009$	–	–	296	–
Gierczak et al. (1997) <sup>c</sup>	$1.09 \pm 0.05$	0	$49 \pm 11$	[220,415]	$1.25 \pm 0.07$
DeMore (1993) <sup>a</sup>	0.91	0	75	[298,360]	1.17
Gordon and Mulac (1975) <sup>d</sup>	1.50	–	–	416	–
Gordon and Mulac (1975) <sup>d,i</sup>	1.06	–	–	416	–
Theoretical studies					
Present study <sup>e</sup>	1.314	0	6.354	[200,300]	1.339
Sellevåg et al. (2006) <sup>f</sup>	[1.30, 1.00]	–	–	[200,1500]	1.27
Masgrau et al. (2001) <sup>g,j</sup>	1.00	-0.02	50.5	[200,1500]	1.25

<sup>a</sup>Fourier transform infrared spectroscopy - relative rate

<sup>b</sup>Tunable diode laser absorption spectroscopy - isotope ratio mass spectrometer

<sup>c</sup>Pulsed photolysis - pulsed laser-induced fluorescence

<sup>d</sup>Pulse radiolysis

<sup>e</sup>Transition state theory with Wigner tunneling correction

<sup>f</sup>Canonical unified statistical theory

<sup>g</sup>Multicoefficient correlation method

<sup>h</sup>Average room temperature value, not obtained from curve fit

<sup>i</sup>Re-evaluated by DeMore (1993)

<sup>j</sup>Arrhenius parameters available at (NIST, 2015)

The present experimental room temperature results for  ${}^D\alpha$  agree, to within the error bars, with the previous experimental studies, with the exception of DeMore (1993). DeMore (1993) used FTIR spectroscopy with a slow flow setup where the two methane isotopologues were measured separately with a common reference compound. The low  ${}^D\alpha$  value in DeMore (1993) may be explained by interference from  $\text{O}({}^1\text{D})$  radicals: OH radicals were produced by photolysis of  $\text{O}_3$  at 254 nm in the presence of  $\text{H}_2\text{O}$ , as in the present study. A relatively high rate of reaction (R3) would reduce the final kinetic isotope effect, since the kinetic isotope effect for oxidation with  $\text{O}({}^1\text{D})$  is smaller than the kinetic isotope effect for the oxidation of OH (Saueressig et al., 2001). The present experimental results of  ${}^D\alpha$  are also in good agreement with Masgrau et al. (2001) and Sellevåg et al. (2006). The theoretical calculations of  ${}^D\alpha$  give a slightly higher value than the experimental results, although they are in good agreement with the best Arrhenius curve fit at  $T = 298\text{K}$ .

**Table 4.** Experimental and theoretical studies of  $^{13}\text{C}\alpha$ . The temperature dependence studies are presented in the Arrhenius form  $^{13}\text{C}\alpha(T) = A \exp(BT^{-1})$ , where  $A$  and  $B$  are tabulated,  $T$  is the given temperature range, and  $^{13}\text{C}\alpha(T = 298\text{K})$  is the resulting kinetic isotope effect at  $T = 298\text{K}$ . Where no  $B$  coefficient is presented  $A$  can be taken as  $^{13}\text{C}\alpha(T)$  for the given temperature range. All uncertainties are given as one standard deviation ( $\sigma$ ).

Study	$A$	$B/\text{K}$	$T/\text{K}$	$^{\text{D}}\alpha(T = 298\text{K})$
Experimental studies				
Saueressig et al. (2001) <sup>a</sup>	$1.0039 \pm 0.0002$	–	296	–
Cantrell et al. (1990) <sup>b</sup>	$1.0054 \pm 0.0005$	–	[273, 353]	$1.0054 \pm 0.0005$
Rust and Stevens (1980) <sup>c,i</sup>	1.003	–	–	–
Theoretical studies				
Present study <sup>d</sup>	1.0137	-1.219	[200,300]	1.0094
Sellekvåg et al. (2006) <sup>e</sup>	[1.014, 1.00]	–	[200,1500]	1.003
Gupta et al. (1997) <sup>f</sup>	1.010	–	300	–
Melissas and Truhlar (1993) <sup>gh</sup>	[1.005, 1.001]	–	[223,416]	1.005
Lasaga and Gibbs (1991) <sup>h</sup>	[1.0036, 1.0076]	–	[150,350]	–

<sup>a</sup>Tunable diode laser absorption spectroscopy - isotope ratio mass spectrometer

<sup>b</sup>Gas chromatography - mass spectrometry

<sup>c</sup>Isotope ratio mass spectrometry

<sup>d</sup>Transition state theory with Wigner tunneling correction

<sup>e</sup>Canonical variational transition state theory

<sup>f</sup>Conventional transition state theory

<sup>g</sup>Interpolated variational transition state theory with centrifugal-dominant, small-curvature tunneling coefficients

<sup>h</sup>Ab initio calculations

<sup>i</sup>No temperature information available

**Table 5.** Experimental and theoretical studies of  $^{13}\text{C,D}\alpha$ . The temperature dependencies are presented in the Arrhenius form  $^{13}\text{C,D}\alpha(T) = A \exp(BT^{-1})$ , where  $A$  and  $B$  are tabulated,  $T$  is the given temperature range, and  $^{13}\text{C,D}\alpha(T = 298\text{K})$  is the resulting kinetic isotope effect at  $T = 298\text{K}$ . All uncertainties are given as one standard deviation ( $\sigma$ ).

Study	$A$	$B/\text{K}$	$T/\text{K}$	$^{\text{D}}\alpha(T = 298\text{K})$
Experimental study <sup>a</sup>	$1.18 \pm 0.10$	$38 \pm 26$	[278,313]	$1.34 \pm 0.03^c$
Theoretical study <sup>b</sup>	1.328	5.301	[200,300]	1.349

<sup>a</sup>Fourier transform infrared spectroscopy - relative rate

<sup>b</sup>Transition state theory with Wigner tunneling correction

<sup>c</sup>Average room temperature value, not obtained from curve fit

The experimental room temperature result for  $^{13}\text{C,D}\alpha = 1.34 \pm 0.03$  agrees to within the error bar with both the theoretical value and the best estimate of the Arrhenius curve fit at  $T = 298\text{K}$ .

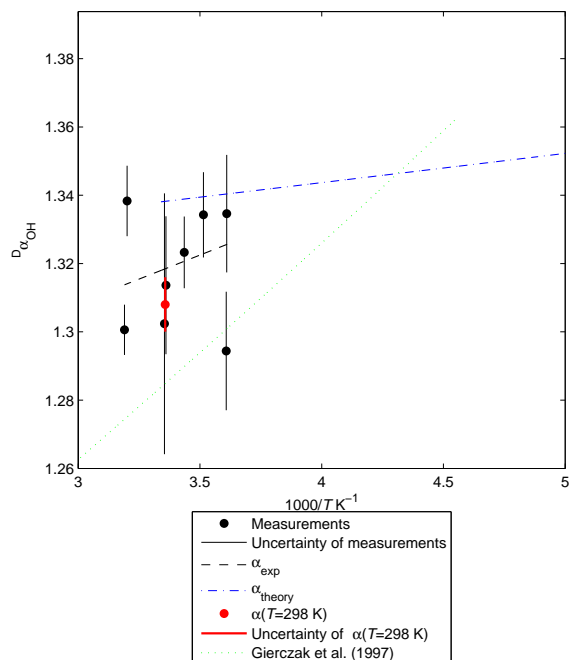


**Figure 5.** The individual measurements of  $^D\alpha$ , are represented by black points; the accompanying individual error bars are represented by thin black solid lines; the experimental Arrhenius curve fit is represented by a black dashed line; the theoretical Arrhenius curve fit is represented by a blue dashed-dotted line; the mean of the room temperature measurements are represented by a red solid circle; the uncertainty of the room temperature measurements are represented by a thick red solid line; the result from Gierczak et al. (1997) (which is included for comparison) are represented by a green dotted line. All uncertainties are given as one standard deviation ( $\sigma$ ).

The theoretical calculations show a very small temperature dependence; the variability in the experimental data is large compared to the value of the slope, making a quantification of the temperature dependence uncertain. Furthermore, the theoretical analysis revealed that the primary cause for the kinetic isotope effect is the substantially reduced reactivity of the D atom, which, in turn, can be explained by a significant increase in reaction barrier due to changes in vibrational zero point energy and to a lesser extent tunneling.

#### 4.1 Atmospheric implications

At steady state, assuming no clumping in emissions,  $\Delta(^{13}\text{CH}_3\text{D}) = \ln(\gamma)$ . It follows that  $\Delta(^{13}\text{CH}_3\text{D}) = 0.02 \pm 0.02$  implying that the clumped isotope effect of the OH reaction is very small. In turn, this implies that the bulk tropospheric  $\Delta(^{13}\text{CH}_3\text{D})$  reflects the source signal with relatively small ad-

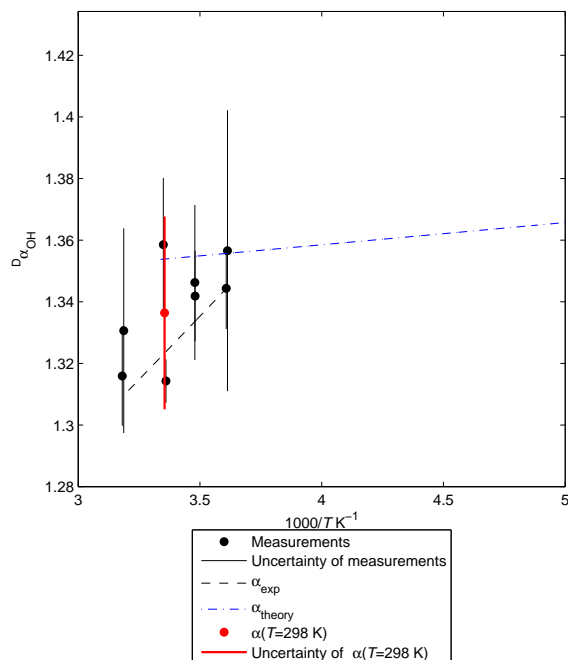


**Figure 6.** The individual measurements of  $^{13}\text{C,D}\alpha$ , are represented by black points; the accompanying individual error bars are represented by thin black solid lines; the experimental Arrhenius curve fit is represented by a black dashed line; the theoretical Arrhenius curve fit is represented by a blue dashed-dotted line; the mean of the room temperature measurements are represented by a red solid circle; the uncertainty of the room temperature measurements are represented by a thick red solid line. All uncertainties are given as one standard deviation ( $\sigma$ ).

justment due to the sink signal (i.e. mainly OH oxidation).  $\Delta(^{13}\text{CH}_3\text{D})$  would therefore be a more straightforward tracer for tracking methane sources than conventional isotopic analysis. However, the present uncertainty overrides the current estimated methane source signals (Wang et al., 2015), thus more precise measurements are necessary.

## 260 5 Conclusions

We present experimentally derived  $\text{CH}_4 + \text{OH}$  kinetic isotope effects and their temperature dependence for  $\text{CH}_3\text{D}$  and  $^{13}\text{CH}_3\text{D}$ ; the latter is reported for the first time. We find  $^{\text{D}}\alpha = 1.31 \pm 0.01$  and  $^{13}\text{C,D}\alpha = 1.34 \pm 0.03$  at room temperature, implying that the kinetic isotope effect is multiplicative such that  $(k_{\text{CH}_4}/k_{^{13}\text{CH}_4})(k_{\text{CH}_4}/k_{\text{CH}_3\text{D}}) = k_{\text{CH}_4}/k_{^{13}\text{CH}_3\text{D}}$  to within the experimental uncertainty.

265 We compare our experimental results to theoretical estimates derived using transition state theory with tunneling correction and kinetic isotope effects reported in the literature. We find good agree-

ment between theoretical and literature values. Based on these experiments we find that the OH reaction (the main sink of methane) at steady-state has a clumped  $\Delta(^{13}\text{CH}_3\text{D}) = 0.02 \pm 0.02$ .

*Acknowledgements.* This research has recieved funding from the European Community's Seventh Framework Programme (FP7/2007-2013) under grant agrement No. 237890, the Carlsberg foundation, and the Danish Council for Independent Research.



## References

- Allan, W., Lowe, D., and Cainey, J.: Active chlorine in the remote marine boundary layer: Modeling anomalous measurements of  $\delta^{13}\text{C}$  in methane, *Geophysical research letters*, 28, 3239–3242, 2001a.
- 275 Allan, W., Manning, M., Lassey, K., Lowe, D., and Gomez, A.: Modeling the variation of  $\delta^{13}\text{C}$  in atmospheric methane: Phase ellipses and the kinetic isotope effect, *Global biogeochemical cycles*, 15, 467–481, 2001b.
- Bergamaschi, P., Bräunlich, M., Marik, T., and Brenninkmeijer, C. A.: Measurements of the carbon and hydrogen isotopes of atmospheric methane at Izaña, Tenerife: Seasonal cycles and synoptic-scale variations, *Journal of Geophysical Research: Atmospheres*, 105, 14 531–14 546, 2000.
- 280 Cantrell, C., Shetter, R., McDaniel, A., Calvert, J., Davidson, J., Lowe, D., Tyler, S., Cicerone, R., and Greenberg, J.: Carbon Kinetic Isotope Effect in the Oxidation of Methane by the Hydroxyl Radical, *J. Geophys. Res.*, 95, 22 455–22 462, 1990.
- Ciais, P., Sabine, C., Bala, G., Bopp, L., Brovkin, V., Canadell, J., Chhabra, A., DeFries, R., Galloway, J., Heimann, M., Jones, C., Le Quéré, C., Myneni, R., Piao, S., and Thornton, P.: Carbon and Other Biogeochemical Cycles. In: *Climate Change 2013: The Physical Science Basis. Contribution of Working Group I to the Fifth Assessment Report of the Intergovernmental Panel on Climate Change*, Cambridge University Press, Cambridge, United Kingdom and New York, NY, USA, 2013.
- 285 Crowley, J. N., Saueressig, G., Bergamaschi, P., Fischer, H., and Harris, G. W.: Carbon kinetic isotope effect in the reaction  $\text{CH}_4 + \text{Cl}$ : a relative rate study using FTIR spectroscopy, *Chem. Phys. Lett.*, 303, 268–274, 1999.
- 290 DeMore, W.: Rate constant ratio for the reactions of OH with  $\text{CH}_3\text{D}$  and  $\text{CH}_4$ , *Journal of physical chemistry*, 97, 8564–8566, 1993.
- Dunning Jr., T. H.: Gaussian basis sets for use in correlated molecular calculations. I. The atoms boron through neon and hydrogen, *J. Chem. Phys.*, 90, 1007–1023, 1989.
- 295 Eiler, J. M., Clog, M., Magyar, P., Piasecki, A., Sessions, A., Stolper, D., Deerberg, M., Schlueter, H. J., and Schwieters, J.: A high-resolution gas-source isotope ratio mass spectrometer, *International Journal of Mass Spectrometry*, 335, 45–56, 2013.
- Feilberg, K. L., Griffith, D. W. T., Johnson, M. S., and Nielsen, C. J.: The  $^{13}\text{C}$  and D kinetic isotope effects in the reaction of  $\text{CH}_4$  with Cl, *Int. J. Chem. Kinet.*, 37, 110–118, 2005.
- 300 Ferretti, D. F., Miller, J. B., White, J. W. C., Etheridge, D. M., Lassey, K. R., Lowe, D. C., Meure, C. M. M., Dreier, M. F., Trudinger, C. M., van Ommen, T. D., and Langenfelds, R. L.: Unexpected changes to the global methane budget over the past 2000 years, *Science*, 309, 1714–1717, 2005.
- Frisch, M. J., Trucks, G. W., Schlegel, H. B., Scuseria, G. E., Robb, M. A., Cheeseman, J. R., Scalmani, G., Barone, V., Mennucci, B., Petersson, G. A., Nakatsuji, H., Caricato, M., Li, X., Hratchian, H. P., Izmaylov, 305 A. F., Bloino, J., Zheng, G., Sonnenberg, J. L., Hada, M., Ehara, M., Toyota, K., Fukuda, R., Hasegawa, J., Ishida, M., Nakajima, T., Honda, Y., Kitao, O., Nakai, H., Vreven, T., Montgomery, Jr., J. A., Peralta, J. E., Ogliaro, F., Bearpark, M., Heyd, J. J., Brothers, E., Kudin, K. N., Staroverov, V. N., Kobayashi, R., Normand, J., Raghavachari, K., Rendell, A., Burant, J. C., Iyengar, S. S., Tomasi, J., Cossi, M., Rega, N., Millam, J. M., Klene, M., Knox, J. E., Cross, J. B., Bakken, V., Adamo, C., Jaramillo, J., Gomperts, R., 310 Stratmann, R. E., Yazyev, O., Austin, A. J., Cammi, R., Pomelli, C., Ochterski, J. W., Martin, R. L., Morokuma, K., Zakrzewski, V. G., Voth, G. A., Salvador, P., Dannenberg, J. J., Dapprich, S., Daniels, A. D.,

- Farkas, O., Foresman, J. B., Ortiz, J. V., Cioslowski, J., and Fox, D. J.: Gaussian 09 Revision A.1, gaussian Inc. Wallingford CT 2009, 2009.
- 315 Gierczak, T., Talukdar, R. K., Herndon, S. C., Vaghjiani, G. L., and Ravishankara, A. R.: Rate Coefficients  
for the Reactions of Hydroxyl Radicals with Methane and Deuterated Methanes, *J. Phys. Chem. A*, 101,  
3125–3134, 1997.
- Gordon, S. and Mulac, W. A.: Reaction of OH(X<sub>2</sub>-PI) radical produced by pulse-radiolysis of water-vapor,  
*International Journal of Chemical Kinetics*, 1, 289–299, 1975.
- 320 Griffith, D., Deutscher, N., Caldow, C., Kettlewell, G., Riggensbach, M., and Hammer, S.: A Fourier transform  
infrared trace gas analyser for atmospheric applications, *Atmospheric Measurement Techniques Discussions*,  
5, 3717–3769, 2012.
- Griffith, D. W. T.: Synthetic Calibration and Quantitative Analysis of Gas-Phase FT-IR Spectra, *Appl. Spec-*  
*trosc.*, 50, 59–70, 1996.
- Gupta, M. L., McGrath, M. P., Cicerone, R. J., Rowland, F. S., and Wolfsberg, M.: C-12/C-13 kinetic isotope  
325 effects in the reactions of CH<sub>4</sub> with OH and Cl, *Geophysical Research Letters*, 24, 2761–2764, 1997.
- Halkier, A., T., H., Jørgensen, P., Klopper, W., Koch, H., Olsen, J., and Wilson, A. K.: Basis-set convergence in  
correlated calculations on Ne, N<sub>2</sub>, and H<sub>2</sub>O, *Chem. Phys. Lett.*, 286, 243 – 252, 1998.
- Ianni, J.: A Comparison of the Bader-Deuflhard and the Cash-Karp Runge-Kutta Integrators for the GRI-MECH  
3.0 Model Base on the Chemical Kinetics Code Kintecus, 2003.
- 330 IPCC: Climate Change 2013: The Physical Science Basis. Contribution of Working Group I to the Fifth Assess-  
ment Report of the Intergovernmental Panel on Climate Change, Cambridge University Press, Cambridge,  
United Kingdom and New York, NY, USA, 2013.
- Joelsson, L. M. T., Forecast, R., Schmidt, J. A., Meusinger, C., Nilsson, E. J. K., Ono, S., and Johnson, M. S.:  
Relative rate study of the kinetic isotope effect in the (CH<sub>3</sub>D)-C-13 + Cl reaction, *Chemical Physics Letters*,  
335 605, 152–157, 2014.
- Kirschke, S., Bousquet, P., Ciais, P., Saunois, M., Canadell, J. G., Dlugokencky, E. J., Bergamaschi, P.,  
Bergmann, D., Blake, D. R., Bruhwiler, L., et al.: Three decades of global methane sources and sinks, *Nature*  
*Geoscience*, 6, 813–823, 2013.
- Knowles, P. J., Hampel, C., and Werner, H.-J.: Coupled cluster theory for high spin, open shell reference wave  
340 functions, *J. Chem. Phys.*, 99, 5219–5227, 1993.
- Knowles, P. J., Hampel, C., and Werner, H.-J.: Erratum: “Coupled cluster theory for high spin, open shell  
reference wave functions” [ *J. Chem. Phys.* 99, 5219 (1993)], *J. Chem. Phys.*, 112, 3106–3107, 2000.
- Lasaga, A. C. and Gibbs, G.: Ab initio studies of the kinetic isotope effect of the CH<sub>4</sub> + OH• atmospheric  
reaction, *Geophysical Research Letters*, 18, 1217–1220, 1991.
- 345 Lassey, K. R., Etheridge, D. M., Lowe, D. C., Smith, A. M., and Ferretti, D. F.: Centennial evolution of the  
atmospheric methane budget: what do the carbon isotopes tell us?, *Atmos. Chem. and Phys.*, 7, 2119–2139,  
2007.
- Liu, Q. and Liu, Y.: Clumped-isotope signatures at equilibrium of CH<sub>4</sub>, NH<sub>3</sub>, H<sub>2</sub>O, H<sub>2</sub>S and SO<sub>2</sub>,  
*Geochimica et Cosmochimica Acta*, 175, 252–270, 2016.

- 350 Lowe, D. C., Manning, M. R., Brailsford, G. W., and Bromley, A. M.: The 1991-1992 atmospheric methane anomaly: Southern Hemisphere C-13 decrease and growth rate fluctuations, *Geophys. Res. Lett.*, 24, 857–860, 1997.
- Ma, Q., Wu, S., and Tang, Y.: Formation and abundance of doubly-substituted methane isotopologues ((CH<sub>3</sub>D)-C-13) in natural gas systems, *Geochim. Cosmochim. Acta*, 72, 5446–5456, 2008.
- 355 Masgrau, L., Gonzalez-Lafont, A., and Lluch, J. M.: The reactions CH<sub>n</sub>D<sub>4-n</sub> + OH → P and CH<sub>4</sub> + OD → CH<sub>3</sub> + HOD as a test of current direct dynamics multicoefficient methods to determine variational transition state rate constants. II, *Journal of Chemical Physics*, 115, 4515–4526, 2001.
- Melissas, V. S. and Truhlar, D. G.: Deuterium and C-13 kinetic isotope effects for the reaction of OH with CH<sub>4</sub>, *Journal of Chemical Physics*, 99, 3542–3552, 1993.
- 360 Møller, C. and Plesset, M. S.: Note on an Approximation Treatment for Many-Electron Systems, *Phys. Rev.*, 46, 618–622, 1934.
- Nilsson, E. J. K., Eskebjerg, C., and Johnson, M. S.: A photochemical reactor for studies of atmospheric chemistry, *Atmospheric Environment*, 43, 3029–3033, 2009.
- Nilsson, E. J. K., Andersen, V. F., Nielsen, O. J., and Johnson, M. S.: Rate coefficients for the chemical reactions of CH<sub>2</sub>F<sub>2</sub>, CHClF<sub>2</sub>, CH<sub>2</sub>FCF<sub>3</sub> and CH<sub>3</sub>CCl<sub>3</sub> with O(<sup>1</sup>D) at 298 K, *Chemical Physics Letters*, 554, 27–32, 2012.
- 365 NIST: National Institute of Standards and Technology Chemical Kinetics Database, <http://kinetics.nist.gov>, last access: 2 October 2015, 2015.
- Ono, S., Wang, D. T., Gruen, D. S., Sherwood Lollar, B., Zahniser, M. S., McManus, B. J., and Nelson, D. D.: Measurement of a Doubly Substituted Methane Isotopologue, <sup>13</sup>CH<sub>3</sub>D, by Tunable Infrared Laser Direct Absorption Spectroscopy, *Analytical chemistry*, 86, 6487–6494, 2014.
- 370 Pohlman, J., Kaneko, M., Heuer, V., Coffin, R., and Whiticar, M.: Methane sources and production in the northern Cascadia margin gas hydrate system, *Earth and Planetary Science Letters*, 287, 504–512, 2009.
- Quay, P., Stutsman, J., Wilbur, D., Snover, A., Dlugokencky, E., and Brown, T.: The isotopic composition of atmospheric methane, *Global Biogeochemical Cycles*, 13, 445–461, 1999.
- 375 Rothman, L. S., Gordon, I. E., Barbe, A., Benner, Bernath, P. F., Birk, M., Boudon, V., Brown, L. R., Campargue, A., and Champion, J. P.: The HITRAN 2008 molecular spectroscopic database, *J. Quant. Spec. and Rad. Trans.*, 110, 533–572, 2009.
- Rust, F. and Stevens, C.: Carbon kinetic isotope effect in the oxidation of methane by hydroxyl, *International Journal of Chemical Kinetics*, 12, 371–377, 1980.
- 380 Sander, S. P., Friedl, R., Barker, J., Golden, D., Kurylo, M., Moortgat, G., Wine, P., Abbatt, J., Burkholder, J., Kolb, C., Moortgat, G., Huie, R., VL, O., et al.: Chemical kinetics and photochemical data for use in atmospheric studies: evaluation number 17, National Aeronautics and Space Administration, Jet Propulsion Laboratory, California Institute of Technology Pasadena, CA, 2010.
- 385 Saueressig, G., Bergamaschi, P., Crowley, J. N., Fischer, H., and Harris, G. W.: Carbon kinetic isotope effect in the reaction of CH<sub>4</sub> with Cl atoms, *Geophys. Res. Lett.*, 22, 1225–1228, 1995.
- Saueressig, G., Bergamaschi, P., Crowley, J. N., Fischer, H., and Harris, G. W.: D/H kinetic isotope effect in the reaction CH<sub>4</sub> + Cl, *Geophys. Res. Lett.*, 23, 3619–3622, 1996.

- Saueressig, G., Crowley, J. N., Bergamaschi, P., Bruhl, C., Brenninkmeijer, C. A. M., and Fischer, H.: Carbon  
390 <sup>13</sup> and D kinetic isotope effects in the reactions of CH<sub>4</sub> with O(D-1) and OH: New laboratory measurements  
and their implications for the isotopic composition of stratospheric methane, *J. Geophys. Res.-Atmos.*, 106,  
23 127–23 138, 2001.
- Schmidt, J. A. and Johnson, M. S.: Clumped isotope perturbation in tropospheric nitrous oxide from strato-  
spheric photolysis, *Geophysical Research Letters*, 42, 3546–3552, 2015.
- 395 Schmidt, J. A., Johnson, M. S., and Schinke, R.: Carbon dioxide photolysis from 150 to 210 nm: Singlet and  
triplet channel dynamics, UV-spectrum, and isotope effects, *Proceedings of the National Academy of Sci-  
ences*, 110, 17 691–17 696, 2013.
- Sellevåg, S. R., Nyman, G., and Nielsen, C. J.: Study of the carbon-13 and deuterium kinetic isotope effects in  
the Cl and OH reactions of CH<sub>4</sub> and CH<sub>3</sub>Cl, *Journal of Physical Chemistry A*, 110, 141–152, 2006.
- 400 Stolper, D. A., Sessions, A. L., Ferreira, A. A., Santos Neto, E. V., Schimmelmann, A., Shusta, S. S., Valentine,  
D. L., and Eiler, J. M.: Combined C-13-D and D-D clumping in methane: Methods and preliminary results,  
*Geochimica Et Cosmochimica Acta*, 126, 169–191, 2014.
- Tyler, S. C., Rice, A. L., and Ajje, H. O.: Stable isotope ratios in atmospheric CH<sub>4</sub>: Implications for seasonal  
sources and sinks, *J. Geophys. Res.-Atmos.*, 112, 2007.
- 405 Wang, D. T., Gruen, D. S., Lollar, B. S., Hinrichs, K.-U., Stewart, L. C., Holden, J. F., Hristov, A. N., Pohlman,  
J. W., Morrill, P. L., Koenneke, M., Delwiche, K. B., Reeves, E. P., Sutcliffe, C. N., Ritter, D. J., Seewald,  
J. S., McIntosh, J. C., Hemond, H. F., Kubo, M. D., Cardace, D., Hoehler, T. M., and Ono, S.: Nonequilibrium  
clumped isotope signals in microbial methane, *Science*, 348, 428–431, 2015.
- Watts, J. D., Gauss, J., and Bartlett, R. J.: Coupled-cluster methods with noniterative triple excitations for  
410 restricted open-shell Hartree–Fock and other general single determinant reference functions. Energies and  
analytical gradients, *J. Chem. Phys.*, 98, 8718–8733, 1993.
- Wigner, E.: On the quantum correction for thermodynamic equilibrium, *Physical Review*, 40, 749, 1932.
- Woon, D. E. and Dunning Jr., T. H.: Gaussian basis sets for use in correlated molecular calculations. III. The  
atoms aluminum through argon, *J. Chem. Phys.*, 98, 1358–1371, 1993.
- 415 York, D., Evensen, N. M., Martínez, M. L., and De Basable Delgado, J.: Unified equations for the slope, inter-  
cept, and standard errors of best straight line, *Am. J. Phys.*, 72, 367–375, 2004.